

RESEARCH ARTICLE

Fossil leaf wax hydrogen isotopes reveal variability of Atlantic and Mediterranean climate forcing on the southeast Iberian Peninsula between 6000 to 3000 cal. BP

Julien Schirrmacher^{1,2*}, Nils Andersen², Ralph R. Schneider^{1,2,3}, Mara Weinelt¹

1 CRC1266, Christian-Albrechts University, Kiel, Germany, **2** Leibniz Laboratory for Radiometric Dating and Stable Isotope Research, Christian-Albrechts University, Kiel, Germany, **3** Institute of Geosciences, Christian-Albrechts University, Kiel, Germany

* jschirrmacher@leibniz.uni-kiel.de**OPEN ACCESS**

Citation: Schirrmacher J, Andersen N, Schneider RR, Weinelt M (2020) Fossil leaf wax hydrogen isotopes reveal variability of Atlantic and Mediterranean climate forcing on the southeast Iberian Peninsula between 6000 to 3000 cal. BP. PLoS ONE 15(12): e0243662. <https://doi.org/10.1371/journal.pone.0243662>

Editor: Peter F. Biehl, University at Buffalo - The State University of New York, UNITED STATES

Received: July 1, 2020

Accepted: November 24, 2020

Published: December 23, 2020

Copyright: © 2020 Schirrmacher et al. This is an open access article distributed under the terms of the [Creative Commons Attribution License](https://creativecommons.org/licenses/by/4.0/), which permits unrestricted use, distribution, and reproduction in any medium, provided the original author and source are credited.

Data Availability Statement: All files containing compound-specific isotope data from sediment core ODP-161-976A are available from the PANGAEA database (<https://doi.org/10.1594/PANGAEA.919703>).

Funding: This research was performed in the framework of the CRC 1266 “Scales of transformation” (project number: 2901391021) funded by the DFG (German Research Foundation).

Abstract

Many recently published papers have investigated the spatial and temporal manifestation of the 4.2 ka BP climate event at regional and global scales. However, questions with regard to the potential drivers of the associated climate change remain open. Here, we investigate the interaction between Atlantic and Mediterranean climate forcing on the south-eastern Iberian Peninsula during the mid- to late Holocene using compound-specific hydrogen isotopes from fossil leaf waxes preserved in marine sediments. Variability of hydrogen isotope values in the study area is primarily related to changes in the precipitation source and indicates three phases of increased Mediterranean sourced precipitation from 5450 to 5350 cal. BP, from 5150 to 4300 cal. BP including a short-term interruption around 4800 cal. BP, and from 3400 to 3000 cal. BP interrupted around 3200 cal. BP. These phases are in good agreement with times of prevailing positive modes of the North Atlantic Oscillation (NAO) and reduced storm activity in the Western Mediterranean suggesting that the NAO was the dominant modulator of relative variability in precipitation sources. However, as previously suggested other modes such as the Western Mediterranean Oscillation (WeMO) may have altered this overall relationship. In this regard, a decrease in Mediterranean moisture source coincident with a rapid reduction in warm season precipitation during the 4.2 ka BP event at the south-eastern Iberian Peninsula might have been related to negative WeMO conditions.

Introduction

In recent years much effort has been made in reconstructing and understanding the socio-environmental dynamics associated with the 4.2 ka BP event. Initially, the 4.2 ka BP event was described as an “archaeological event” in the Near East, where the Akkadian Empire potentially collapsed due to an increase in regional aridity [1]. Similar climatic related collapses or transformations within ancient societies at that time have also been documented in different regions across the northern hemisphere [2–4] including southern Iberia [5, 6]. However, regional heterogeneity in both, climatic conditions and social developments, have been

Competing interests: The authors have declared that no competing interests exist.

indicated within the Mediterranean region [6–8]. Still, the narrative of a megadrought affecting ancient societies across Asia, the Mediterranean, and northeast Africa arose [9, 10].

Such a first evidence of climate related collapses or transformations in ancient societies have promoted intense investigations of the “climatic” 4.2 ka BP event, which resulted in a variety of associated paleoclimatic studies from the Mediterranean area [6, 7, 11, 12], Asia [13–15], North America [16], the northern North Atlantic region [17–19], and the southern hemisphere as well [20, 21]. Altogether, paleoclimatic studies point to a series of climatic anomalies between 4400 and 3800 cal. BP, which across the Mediterranean region are often registered as dry and cool events [6, 7]. But, climatic conditions may have been variable on a regional and seasonal scale with humid conditions prevailing occasionally [6, 11, 22].

However, potential drivers of the more widespread drier and cooler climate periods across the mid-latitudes of the northern hemisphere are not yet understood. Since the North Atlantic Oscillation (NAO) is modulating winter precipitation across large parts of the Mediterranean region, in particular the Western Mediterranean [23, 24], it is often regarded as one important driver for drought associated with the 4.2 ka BP event [11, 25, 26]. At that time, a major NAO-like forcing is also suggested by modelling studies [27]. On the other hand, recent studies have indicated that the 4.2 ka BP event in the Mediterranean region could have been more pronounced during the summer season [6, 7, 28]. Thus, the search for a potential driver of the climatic 4.2 ka BP event particularly in the Western Mediterranean region has to include seasonal variability with Atlantic winter versus Mediterranean summer forcing.

To shed further light on the potential driver of climate variability around 4200 cal. BP, we investigated the temporal variability of the interaction between Atlantic and Mediterranean climatic regimes. Therefore, we analysed compound-specific hydrogen and carbon isotopes from fossil leaf waxes, i.e. land-derived *n*-alkanes, as tracer of past atmospheric circulation patterns in a well-suited marine sediment core from the Alboran Sea—an area actually located at the interface of Atlantic and Mediterranean climate regimes (Fig 1).

Study area

The terrestrial organic compounds investigated in this study are mainly sourced from the catchment areas of the Guadiaro and Guadalhorce rivers (Fig 1). Both catchment areas are draining the Thermo- and Mesomediterranean vegetation belts (Fig 1). These vegetation belts in the southern Iberian Peninsula are generally characterized by scrubland and grassland with only patchy forests in favourable locations such as water courses [29]. While the main tree species are different *Quercus* species, water courses are dominated by *Salix*, *Fraxinus*, and *Ulmus* [29]. Important shrub species in the study area are *Juniperus*, *Phillyrea*, *Erica*, *Olea*, and *Arbutus unedo* [29].

Most of the aforementioned species are adapted to the high seasonality in the study area, which is currently under a Mediterranean climate influence characterized by a cool and rainy winter season and a hot and dry summer season. Based on data from the Spanish State Meteorological Agency (AEMET) modern (1981–2010) winter conditions in the study area range between a minimum air temperature of 12.1°C at Málaga airport and 13.0°C at Tarifa close to Gibraltar. At these stations, precipitation reveals a maximum during winter of up to 100 and 118 mm at Málaga and Tarifa stations, respectively. In contrast, summer conditions are characterized by maximum temperatures between 22.3 and 26.0°C at Tarifa and Málaga stations. Between June and August there is almost no precipitation occurring at both stations.

The temporal variability of precipitation in the study area is mainly controlled by the North Atlantic Oscillation (NAO), which primarily transports moisture from the Atlantic during the winter season [24, 43, 44]. During positive NAO (NAO⁺; i.e. a high difference in sea level

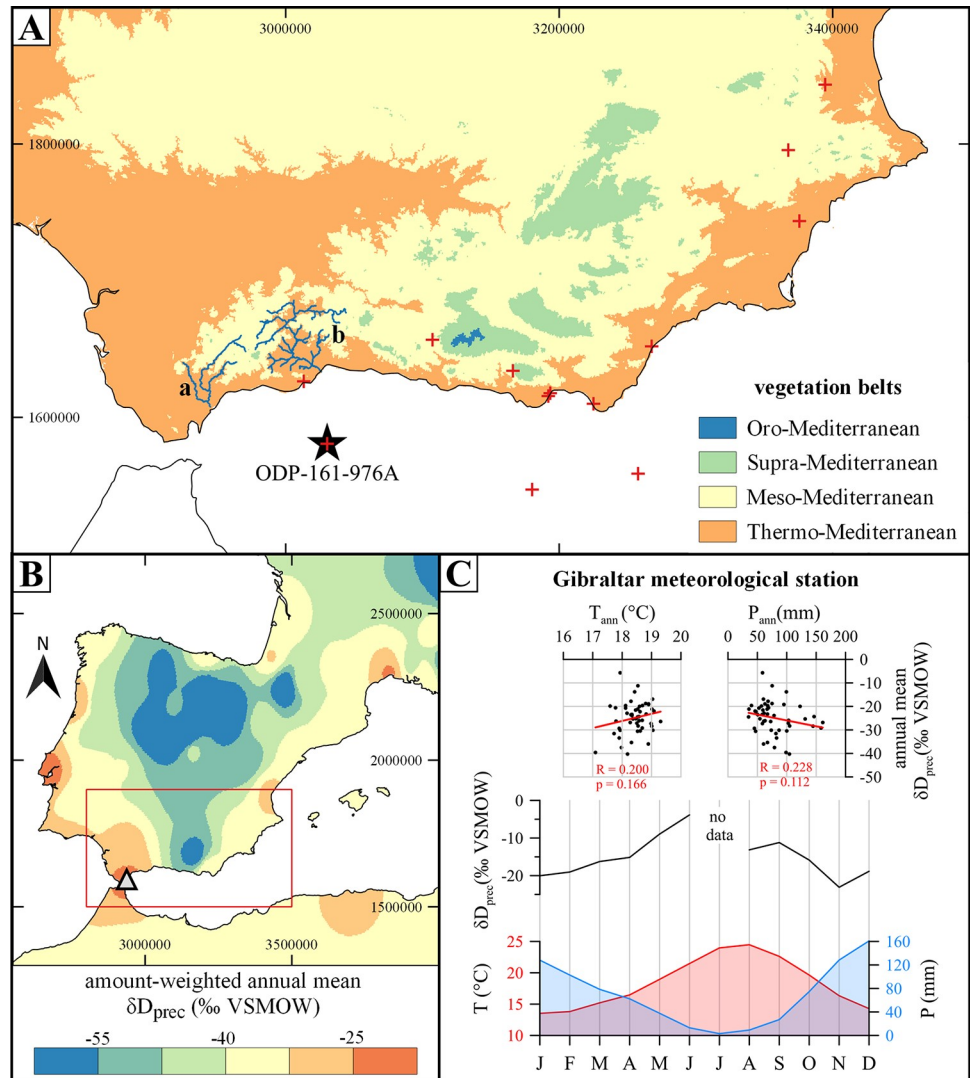


Fig 1. Study area. A) Major vegetation belts at the south-eastern Iberian Peninsula are shown along with main rivers Guadiaro (a) and Guadalhorce (b) in the study area. Vegetation belts have been calculated after [29] based on 0.5° gridded climate data from WorldClim V2.0 [30]. Star indicates the location of marine sediment core ODP-161-976A and red crosses show locations of additional archives used for regional paleoclimatological analysis (see Table 1 for more detailed information): Navarrés [31], Villena [32], Elx [33], Antas [34], Padul [26], Sierra de Gádor [35], Roquetas de Mar [34], San Rafael [34], Cabo de Gata [36], El Refugio [37], TTR14-300G [38], ODP-161-976A [11, 39] and, MD95-2043 [7, 40–42]. B) Map showing the spatial distribution of amount-weighted long-term (1961–2016) annual mean hydrogen isotopic composition of precipitation (δD_{prec}). The raw data was downloaded from the Global Network of Isotopes in Precipitation (GNIP) database and interpolated using an inverse distance weighted (IDW) approach (unlimited search radius and power value = 3.0). Red square indicates area shown in A). Triangle denotes the location of Gibraltar meteorological station, which data is shown to the right. C) Average monthly air temperature (T), precipitation (P) and, amount-weighted δD_{prec} of Gibraltar meteorological station for the period 1961–2016 (bottom) as well as the correlation of their annual means (top). All raw data from Gibraltar meteorological station have been downloaded from the GNIP database. Please note, that no δD_{prec} data is available for July due to the scarce precipitation during that month.

<https://doi.org/10.1371/journal.pone.0243662.g001>

pressure between the Azores and Iceland) the study area experiences drier conditions, because the main storm track of the westerlies lead towards northern and central Europe (Fig 2), and *vice versa*. A secondary mode responsible for temporal climate variability in the area is the Western Mediterranean Oscillation (WeMO) [45]. In its positive phase (WeMO⁺) the Western

Table 1. Dataset used for the regional precipitation analysis.

Site	Season	Archive	Proxy	Reference
Antas	annual	terrestrial	Xerophytes	[34]
El Refugio Cave	annual	speleothem	Stalagmite density	[37]
Elx	annual	terrestrial	Xerophytes	[33]
MD95-2043	annual	marine	MAT on pollen	[7, 40–42]
MD95-2043	annual	marine	Xerophytes	[41]
Navarrés	annual	terrestrial	WAPLS on pollen	[31]
ODP-161-976A	annual	marine	MAT on pollen	[6,39]
Padul	annual	terrestrial	Xerophytes	[26]
Roquetas de Mar	annual	terrestrial	Xerophytes	[34]
San Rafael	annual	terrestrial	Xerophytes	[34]
San Rafael	annual	terrestrial	WAPLS on pollen	[31]
Sierra de Gádor	annual	lake	Xerophytes	[35]
TTR14-300G	annual	marine	La/Lu ratio	[38]
ODP-161-976A	annual	marine	ACL ₂₉₋₃₅	this study
Antas	cold season	terrestrial	arboreal pollen	[34]
Cabo de Gata	cold season	terrestrial	arboreal pollen	[36]
Elx	cold season	terrestrial	arboreal pollen	[33]
MD95-2043	cold season	marine	MAT on pollen	[7, 40–42]
MD95-2043	cold season	marine	arboreal pollen	[41]
ODP-161-976A	cold season	marine	MAT on pollen	[6,39]
Padul	cold season	terrestrial	arboreal pollen	[26]
Roquetas de Mar	cold season	terrestrial	arboreal pollen	[34]
San Rafael	cold season	terrestrial	arboreal pollen	[34]
Sierra de Gádor	cold season	lake	arboreal pollen	[35]
Villena	cold season	terrestrial	pollen ratio	[32]
MD95-2043	warm season	marine	MAT on pollen	[7, 40–42]
ODP-161-976A	warm season	marine	MAT on pollen	[6, 39]

MAT = modern analogue technique, WAPLS = weighted-average partial least squares regression technique.

<https://doi.org/10.1371/journal.pone.0243662.t001>

Mediterranean Oscillation is associated with relatively cool and dry north-westerly winds, while during its negative phase (WeMO⁻) relatively warm and humid easterly winds are prevailing (Fig 2). The WeMO is active throughout the year, but WeMO⁻ conditions are particularly associated with increased winter precipitation along the Catalanian and Valencian coasts [45, 46].

The scarce precipitation during the summer season in the study area, when the NAO driven influence is less pronounced [47], is mainly driven by mesoscale synoptic patterns and local convective systems [48]. These are responsible for short torrential rainfall events, which are particularly evident along the Mediterranean coast during times of a high land-sea temperature contrast [48]. Such a high land-sea temperature contrast may be promoted by the advection of cool northerly air masses under WeMO⁺ conditions during summer [46].

Overall, both atmospheric modes—the NAO and the WeMO—modulate the temporal variability of the two main precipitation sources at the Iberian Peninsula, which are an Atlantic source dominant during winter and a Mediterranean source during summer [49]. These two precipitation sources are also reflected in the spatial distribution of the hydrogen isotopic composition within the amount-weighted long-term annual mean precipitation (δD_{prec}). In the Atlantic dominated inland areas amount-weighted annual mean δD_{prec} values are typically

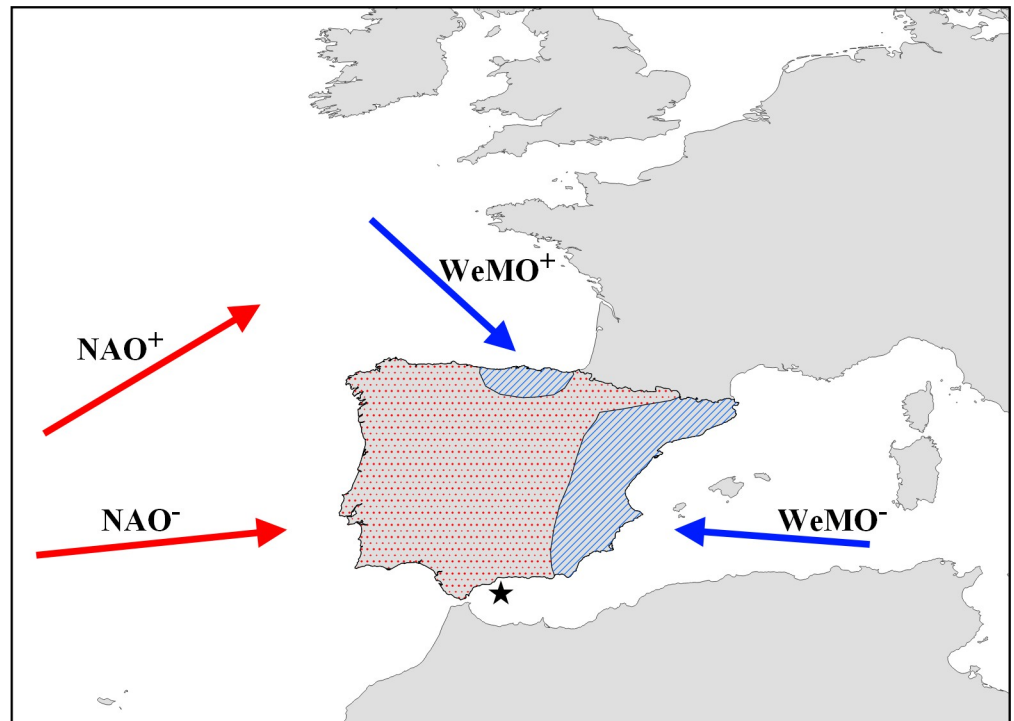


Fig 2. Main atmospheric drivers of temporal precipitation variability on the Iberian Peninsula. Map showing areas on the Iberian Peninsula, where temporal winter (October–March) precipitation variability is dominated by the NAO (dotted red) and the WeMO (hatched blue). Areas have been redrawn from [45]. Red arrows indicate dominant wind direction under NAO⁺ and NAO⁻ conditions, respectively. Blue arrows indicate the same for WeMO⁺ and WeMO⁻ conditions. Star indicates the location of marine sediment core ODP-161-976A.

<https://doi.org/10.1371/journal.pone.0243662.g002>

below -40 ‰ VSMOW, while coastal areas, which are more intensely affected by local precipitation sources, vary between -15 and -35 ‰ VSMOW (Fig 1). Moreover, at Gibraltar meteorological station amount-weighted δD_{prec} values show no significant correlation with precipitation amount or temperature on the annual scale (Fig 1). However, on the monthly scale amount-weighted δD_{prec} values are highly correlated with precipitation amount ($R = 0.849$; $p < 0.001$) and temperature ($R = 0.756$; $p = 0.004$) (not shown). This is because the precipitation source, which generally varies on a seasonal scale (Atlantic winter and Mediterranean summer) [49], might be responsible for the observed seasonal variability of amount-weighted δD_{prec} values in the study area [48].

***n*-Alkane data as paleoclimatic proxy**

n-Alkanes are synthesized by terrestrial plants as leaf waxes in order to protect themselves against water loss due to evapotranspiration [50]. After eolian or riverine transport, leaf waxes are deposited in soils, lakes, and marine sediments [51–53]. After deposition in the sediments, *n*-alkanes are relatively resistant to diagenesis [54, 55] and may serve as paleoclimatic indicator. Potential alteration of *n*-alkanes can be investigated by the carbon preference index (CPI), which illustrates the ratio of odd versus even chain lengths [56]. Usually, a CPI above 2 indicates that *n*-alkanes are not altered and, thus, can be reliably used as paleoclimatic indicator [57]. The average chain length (ACL) of *n*-alkanes might be used as such a paleoclimatic indicator since it has been found to record regional aridity in Mediterranean settings [58, 59]. This is based on the observation, that plants produce on average longer *n*-alkane homologues

resulting in an increasing ACL, when water availability is reduced [60]. Also, isotopic analyses of individual *n*-alkanes, have been used extensively during the last years in tropical [61–64] but also in Mediterranean regions [65–68] in order to assess terrestrial environmental and climatic parameters.

Analysing individual *n*-alkane homologues for carbon isotopes ($\delta^{13}\text{C}_{\text{Cx}}$) provides important information on the distribution of C3 and C4 plants [69]. Due to their different photosynthetic pathway, C4 plants typically exhibit elevated $\delta^{13}\text{C}_{\text{Cx}}$ values varying between -20 to -15 ‰ compared to those from C3 plants, which vary between -45 to -30 ‰ [69, 70]. In environmental settings, which are characterized by stability of the vegetational record with regard to C3 vs. C4 plant distribution, $\delta^{13}\text{C}_{\text{Cx}}$ values may also record plant water stress [71]. Increasing $\delta^{13}\text{C}_{\text{Cx}}$ values would point to isotopic enrichment within the plant's source water pool due to enhanced evapotranspiration. In Mediterranean settings, $\delta^{13}\text{C}_{\text{Cx}}$ data of the long chain *n*-alkanes have been suggested to be most suitable for studying changes in humidity [58].

In settings mixed with C3 and C4 plants, the $\delta^{13}\text{C}_{\text{Cx}}$ values are further needed for potential correction of the hydrogen isotopic data of the individual *n*-alkanes ($\delta\text{D}_{\text{Cx}}$) [72, 73]. Despite of potential alteration through the vegetation type, the $\delta\text{D}_{\text{Cx}}$ data is highly correlated with that of the water source, i.e. precipitation ($\delta\text{D}_{\text{prec}}$) during the plants growing season [74]. Additional factors controlling $\delta\text{D}_{\text{prec}}$ and thus, also $\delta\text{D}_{\text{Cx}}$ are atmospheric temperature, the amount of rainfall, evapotranspiration, and precipitation source [74–76].

Materials and methods

Sediment core and age model

Sediment core ODP-161-976A (36° 12.320' N; 4° 18.760' W; 1108m water depth) was retrieved in the Alboran Sea during the JOIDES RESOLUTION cruise in 1995 [77]. The sampling of this sediment core was already described in a previous paper [11]. To achieve multi-decadal resolution, the section from 100.0 to 149.0 cm was continuously sampled at 0.5 cm distances in the IODP (International Ocean Discovery Program) core repository at MARUM (Center for Marine Environmental Sciences) in Bremen (Germany). Also, the age model of sediment core ODP-161-976A has already been published in earlier publications [6, 11]. The final age model of ODP-161-976A is based on 11 AMS ^{14}C dates. The sediment core encompasses an analysed time period between ca. 5750 to 3000 cal. BP with a temporal resolution varying between 8 and 114 years for ODP-161-976A.

Sample preparation and calculations

The sample preparation of sediment core ODP-161-976A followed the protocol of the biomarker laboratory at Kiel University and has already been described in an earlier study [11]. In short, *n*-alkanes were extracted from the freeze-dried and finely ground sediment samples with an accelerated solvent extractor (ASE-200, Dionex) at 100 bar and 100°C using a 9:1 (v = v) mixture of dichloromethane (DCM) and methanol. After extraction samples were de-sulfured by stirring for 30 minutes with activated copper. The de-sulfured *n*-alkanes were subsequently separated by silica gel column chromatography using activated silica gel and hexane. *n*-Alkanes were further separated using silver nitrate (AgNO_3) coated silica gel. Subsequently, individual *n*-alkane homologues have been identified with an Agilent 6890N gas chromatograph equipped with a Restek XTI-5 capillary column (30 m x 320 μm x 0.25 μm) based on the comparison of their retention times with an external standard containing a series of *n*-alkane homologues of known concentration. On this basis, *n*-alkanes were also quantified using the FID peak areas calibrated against the external standard. The concentrations of odd terrestrial *n*-alkanes are provided in the supplement of this article.

Based on the quantified *n*-alkane concentrations the carbon preference index (CPI) has been calculated in order to assess potential alteration of the sedimentary *n*-alkanes and thus, their reliability as paleoclimatic indicator:

$$\text{CPI}_{27-33} = 0.5 * \left(\frac{(n-C_{27} + n-C_{29} + n-C_{31} + n-C_{33})}{(n-C_{26} + n-C_{28} + n-C_{30} + n-C_{32})} + \frac{(n-C_{27} + n-C_{29} + n-C_{31} + n-C_{33})}{(n-C_{28} + n-C_{30} + n-C_{32} + n-C_{34})} \right) \quad (1)$$

As paleoclimatic indicator the average chain length (ACL) has been calculated following Norström et al. [58]:

$$\text{ACL}_{29-35} = \frac{29 * n-C_{29} + 31 * n-C_{31} + 33 * n-C_{33} + 35 * n-C_{35}}{n-C_{29} + n-C_{31} + n-C_{33} + n-C_{35}} \quad (2)$$

In both equations *n*-C_x refers to the concentration of the *n*-alkane with x carbon atoms.

Compound-specific isotope analysis

For this study, terrestrial-sourced *n*-alkane homologues of sufficient concentration (i.e. *n*-C₂₉, *n*-C₃₁, and *n*-C₃₃) have been analysed by gas chromatography-isotope ratio mass spectrometry (GC-IRMS) for δD and δ¹³C at the Leibniz Laboratory for Radiometric Dating and Stable Isotope Research at Kiel University. Samples have been measured on an Agilent 6890 gas chromatograph equipped with a Gerstel KAS 4 PTV injector and an Agilent DB-5 capillary column (30 m x 250 μm x 0.25 μm) coupled to a Thermo Scientific MAT 253 isotope ratio mass spectrometer (IRMS). Depending on the *n*-alkane concentration, between 5 and 30 μl of each sample has been injected 2–4 times in order to achieve a statistically robust analytical error for each *n*-alkane homologue. The δD and δ¹³C values are reported relative to Vienna Standard Mean Ocean Water (‰ VSMOW) based on Arndt Schimmelmann's A6 reference mixture from 2015 and Vienna Pee Dee Belemnite (‰ VPDB) scales using Arndt Schimmelmann's A7 reference mixture from 2017, respectively.

For final evaluation of the δD and δ¹³C data, their weighted-mean averages (WMAs) of all three individual isotopic records have been calculated according to the following equation:

$$\delta D_{\text{WMA}} = \sum \delta D_x * \left(\frac{n-C_x}{(n-C_{29} + n-C_{31} + n-C_{33})} \right) \quad (3)$$

with δD_x and *n*-C_x representing the hydrogen isotopic value and the concentration of the *n*-alkane with x carbon atoms, respectively. The same equation has been applied to calculate the δ¹³C_{WMA} data.

Regional analysis

The regional analysis of past seasonal precipitation development is based on a compilation of various climatic proxies from speleothems, marine, lacustrine, and terrestrial archives from the Iberian Peninsula published in a previous publication [6]. For this study, this compilation has been regionally subsampled for the Thermo- and Mesomediterranean vegetation belts in the southeast of the Iberian Peninsula providing new analysis on a regional scale. Furthermore, the ACL₂₉₋₃₅ calculated in this study has been included into the compilation. Altogether, 14 records are reflecting annual, 11 records are reflecting cold season, and 2 records are reflecting warm season precipitation variability (Table 1; Fig 1). The interpretational background of the used proxies is explained in detail in a previous publication [6] or in the individual publications listed in Table 1. However, because the majority of archives are based on pollen percentages, in the following their interpretational background is briefly recalled. Based on the

modern relationship between arboreal pollen and cold season precipitation on the Iberian Peninsula [78], we interpreted decreasing arboreal pollen percentages as indicator for decreasing cold season precipitation. This is further in line with the application in other paleoclimatological studies from the area [26, 40]. On the other hand, xerophytic species including Chenopodiaceae, Amaranthaceae, and *Artemisia* have been shown to be indicative of prolonged annual dry periods [79]. Consequently, an increase in xerophytic pollen percentages have been interpreted as indication of dry annual conditions.

The z-scores [80] of all paleoclimatic proxies reflecting either annual, cold, or warm season precipitation have been combined to regional time-series of qualitative precipitation change. Prior to analysis, the speleothem data of El Refugio Cave [37], which has an average temporal resolution of 3 years, has been downscaled to a temporal resolution of 50 years. The calculation of 50-year means prevents the over-representation of this archive in the regional time-series since it had a much higher temporal resolution compared to all other archives. The regional time-series have then been smoothed using a gaussian LOESS smooth with a 2nd order polynomial and a smoothing parameter of 0.2.

Results

The carbon preference index for odd *n*-alkanes between 27 and 33 carbon atoms (CPI_{27-33}) varies around mean of 6.1 with a minimum of 2.9 and a maximum of 8.7 (Fig 3). The average chain length (ACL) has been calculated for odd *n*-alkanes with carbon atoms ranging between 29 and 35. The ACL_{29-35} reveals no long-term trend and varies between 31.2 and 30.6 with a mean of 30.9 (Fig 3).

Carbon and hydrogen isotopic data of three *n*-alkane homologues (*n*-C₂₉, *n*-C₃₁, and *n*-C₃₃) are presented for the period between ca. 5800 and 3000 cal. BP. In this interval, the carbon isotopic values of the *n*-C₂₉ homologue ($\delta^{13}C_{C29}$) vary between -31.4 and -32.3 ‰ (Fig 3). $\delta^{13}C_{C31}$ values vary between -30.5 and -31.7 ‰, while $\delta^{13}C_{C33}$ values range from -29.5 to -31.6 ‰. There is no obvious trend in any of the carbon isotopic time series, but average values progressively increase with increasing chain length. $\delta^{13}C_{C29}$ values exhibit an average of -31.9 ‰, while $\delta^{13}C_{C31}$ values vary around a mean of -31.3 ‰ and $\delta^{13}C_{C33}$ values are on average -30.5 ‰ (Fig 3). The weighted-mean average of the carbon isotopes $\delta^{13}C_{WMA}$ varies between -31.8 and -30.9 ‰ with a mean value of -31.3 ‰ (Fig 3).

Within the studied timespan, the hydrogen isotopic values vary between -137.3 ‰ and -157.5 ‰ for the *n*-C₂₉ homologue (δD_{C29}), between -141.7 ‰ and -160.8 ‰ for δD_{C31} , and between -113.8 ‰ and -139.9 ‰ for δD_{C33} (Fig 3). While the absolute values and the amplitude of δD_{C29} and δD_{C31} are similar, δD_{C33} values are slightly higher and variability is of larger amplitude. Apart from these differences, hydrogen isotopic values of all three homologues reveal a slightly increasing trend and significantly covary in the analysed period (Table 2). Based on the weighted-mean combination of all three δD records, periods of high and low isotopic values can be distinguished in the δD_{WMA} data (Fig 4). High δD_{WMA} values (-144.5 ‰ on average) are evident around 5400, from 5100 to 4300 with a short-term decrease around ca. 4800 cal. BP, from 3400 to 3300, and at 3000 cal. BP. In contrast, low δD_{WMA} values averaging -149.4 ‰ are noticed at 5500, at 5300, and from 4200 to 3400 cal. BP.

Discussion

Drivers of hydrogen isotopic variability

Variability of hydrogen isotopic data from individual *n*-alkane homologues is potentially driven by five major parameters, which are changes in (1) vegetation types, (2) precipitation amount, (3) atmospheric temperature, (4) evapotranspiration, and (5) precipitation source

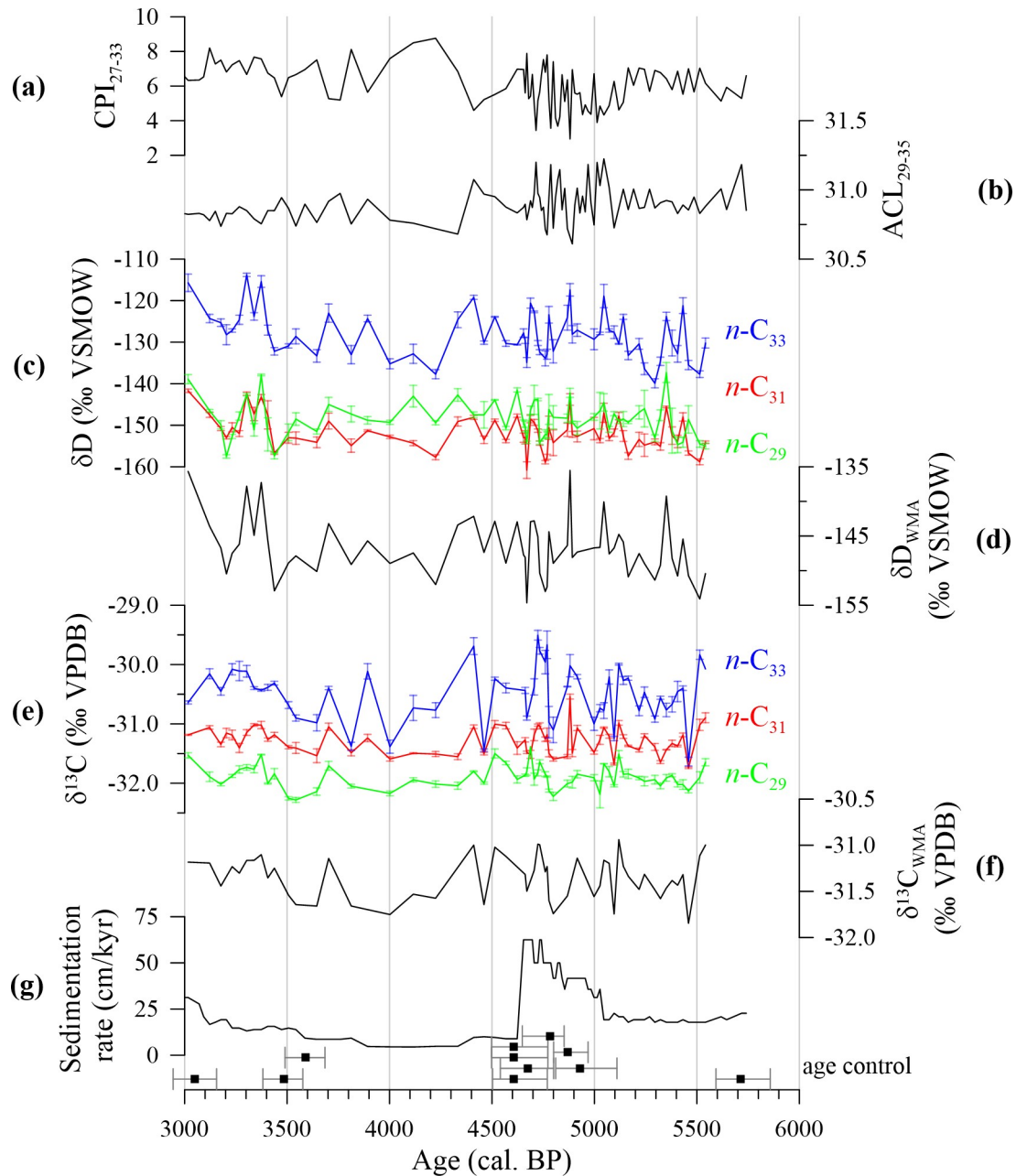


Fig 3. Molecular and isotopic n-alkane data from ODP-161-976A. a) CPI_{27-33} , b) ACL_{29-35} , c) hydrogen isotopic data of individual n-alkane homologues $\delta D_{C_{33}}$ (blue), $\delta D_{C_{31}}$ (red), and $\delta D_{C_{29}}$ (green), d) weighted-mean average of all individual hydrogen isotopic records (δD_{WMA}), e) carbon isotopic data of individual n-alkane homologues $\delta^{13}C_{C_{33}}$ (blue), $\delta^{13}C_{C_{31}}$ (red), and $\delta^{13}C_{C_{29}}$ (green), f) weighted-mean average of all individual carbon isotopic records ($\delta^{13}C_{WMA}$), and g) sedimentation rate. Black squares show calibrated AMS ^{14}C dates and their according uncertainties.

<https://doi.org/10.1371/journal.pone.0243662.g003>

[73–75]. In the following, we conclude that the variability of hydrogen isotopic values from individual n-alkanes originating from southeast Iberia and deposited in marine sediment core ODP-161-976A is primarily driven by changes in the source of precipitation.

Several studies have highlighted the dependence of n-alkane hydrogen isotopic composition on the distribution of C3 and C4 plants in modern [81] and paleoclimatic studies [72, 82, 83]. This is due to the different photosynthetic regulatory pathways of these plant types, which

Table 2. Correlation of carbon and hydrogen isotopic data from ODP-161-976A.

	$\delta^{13}\text{C}_{\text{C31}}$	$\delta^{13}\text{C}_{\text{C33}}$		$\delta\text{D}_{\text{C31}}$	$\delta\text{D}_{\text{C33}}$
$\delta^{13}\text{C}_{\text{C29}}$	R = 0.622	R = 0.540	$\delta\text{D}_{\text{C29}}$	R = 0.856	R = 0.534
	p < 0.001	p < 0.001		p < 0.001	p < 0.001
$\delta^{13}\text{C}_{\text{C31}}$		R = 0.733	$\delta\text{D}_{\text{C31}}$		R = 0.636
		p < 0.001			p < 0.001

<https://doi.org/10.1371/journal.pone.0243662.t002>

results in a different apparent fractionation between the hydrogen isotopic value of precipitation ($\delta\text{D}_{\text{prec}}$) and that of *n*-alkanes ($\delta\text{D}_{\text{Cx}}$) [73]. Any variation in the C3 vs. C4 plant distribution can be tested in parallel through *n*-alkane $\delta^{13}\text{C}$ values. Typically, C4 plants exhibit $\delta^{13}\text{C}_{\text{Cx}}$ values between -20 to -15 ‰, while $\delta^{13}\text{C}_{\text{Cx}}$ values of C3 plants vary between -45 to -30 ‰ [69, 70]. In our case, the similarity and low variability in absolute values for all three compound-specific carbon isotopic data ($\delta^{13}\text{C}_{\text{C29}}$, $\delta^{13}\text{C}_{\text{C31}}$, and $\delta^{13}\text{C}_{\text{C33}}$) in sediment core ODP-161-976A suggest a dominant C3 vegetation cover throughout the entire period (Fig 3). This is in line with various pollen records from southeast Iberia, which show a dominance of C3 vegetation and no major change towards increased C4 vegetation between 6000 and 3000 cal. BP [26, 39, 41]. Furthermore, $\delta^{13}\text{C}$ and δD values within each *n*-alkane homologue, including the weighted-mean average (WMA) isotopic records, are not correlated at a significant level, with the exception of the *n*-C₃₁ homologue revealing a significant but moderate correlation (Table 3). This rules out any significant changes in plant types that may have affected the hydrogen isotopic data at the core site.

Other crucial parameters driving the hydrogen isotopic signal of *n*-alkanes are changes in atmospheric temperature, precipitation amount, and related evapotranspiration [73, 74, 84]. Meteorological data from Gibraltar implies a general connection of $\delta\text{D}_{\text{prec}}$ values to modern changes in the amount of precipitation and atmospheric temperature on a monthly scale (Fig 1). However, no significant statistical correlation of $\delta\text{D}_{\text{prec}}$ values with precipitation amount (R = 0.228, p = 0.112) and atmospheric temperature (R = 0.200, p = 0.166) exists during modern times on the annual scale (Fig 1). Moreover, there is also no significant correlation between all three compound-specific hydrogen isotope records and their concentration as well as with other ODP-161-976A data such as the ACL₂₉₋₃₅ (reflecting changes in regional aridity [58]) and alkenone-based annual mean SST (Table 3), which are closely coupled to atmospheric temperature variability in southeast Iberia [6]. However, correlations between the $\delta\text{D}_{\text{Cx}}$ records appear to increase with chain length (Table 3). Overall, a moderate correlation of ACL₂₉₋₃₅ and the $\delta\text{D}_{\text{WMA}}$ record suggests that regional aridity may have had a minor influence on the hydrogen isotopic records. Aridity is closely related to evapotranspiration, which is potentially an important parameter to be considered, when interpreting $\delta\text{D}_{\text{Cx}}$ data in semi-arid climates such as southeast Iberia. Evapotranspiration can be studied using $\delta^{13}\text{C}$ values, which are claimed to record plant water stress [71, 85]. As noted before, all individual $\delta^{13}\text{C}$ records suggest a constant dominance of C3 plant species, enabling the interpretation of the $\delta^{13}\text{C}_{\text{WMA}}$ record as indicator of plant water stress [71]. We also note, that $\delta^{13}\text{C}_{\text{WMA}}$ values are moderately correlated with ACL₂₉₋₃₅ values (R = 0.442, p = 0.001), further corroborating the use of the $\delta^{13}\text{C}_{\text{WMA}}$ record as recorder of past plant water stress in this study. However, $\delta^{13}\text{C}_{\text{WMA}}$ values are not significantly correlated to $\delta\text{D}_{\text{WMA}}$ values (Table 3) arguing against an influence of plant water stress and further, aridity on the hydrogen isotopic composition within the studied *n*-alkane homologues. Altogether, the ACL₂₉₋₃₅ and $\delta^{13}\text{C}_{\text{WMA}}$ records indicate a minor, if any, influence of aridity and related evapotranspiration on the $\delta\text{D}_{\text{WMA}}$ values.

Thus, we assume that these parameters as well as precipitation amount and atmospheric temperature have not been dominant drivers for the observed *n*-alkane hydrogen variability in

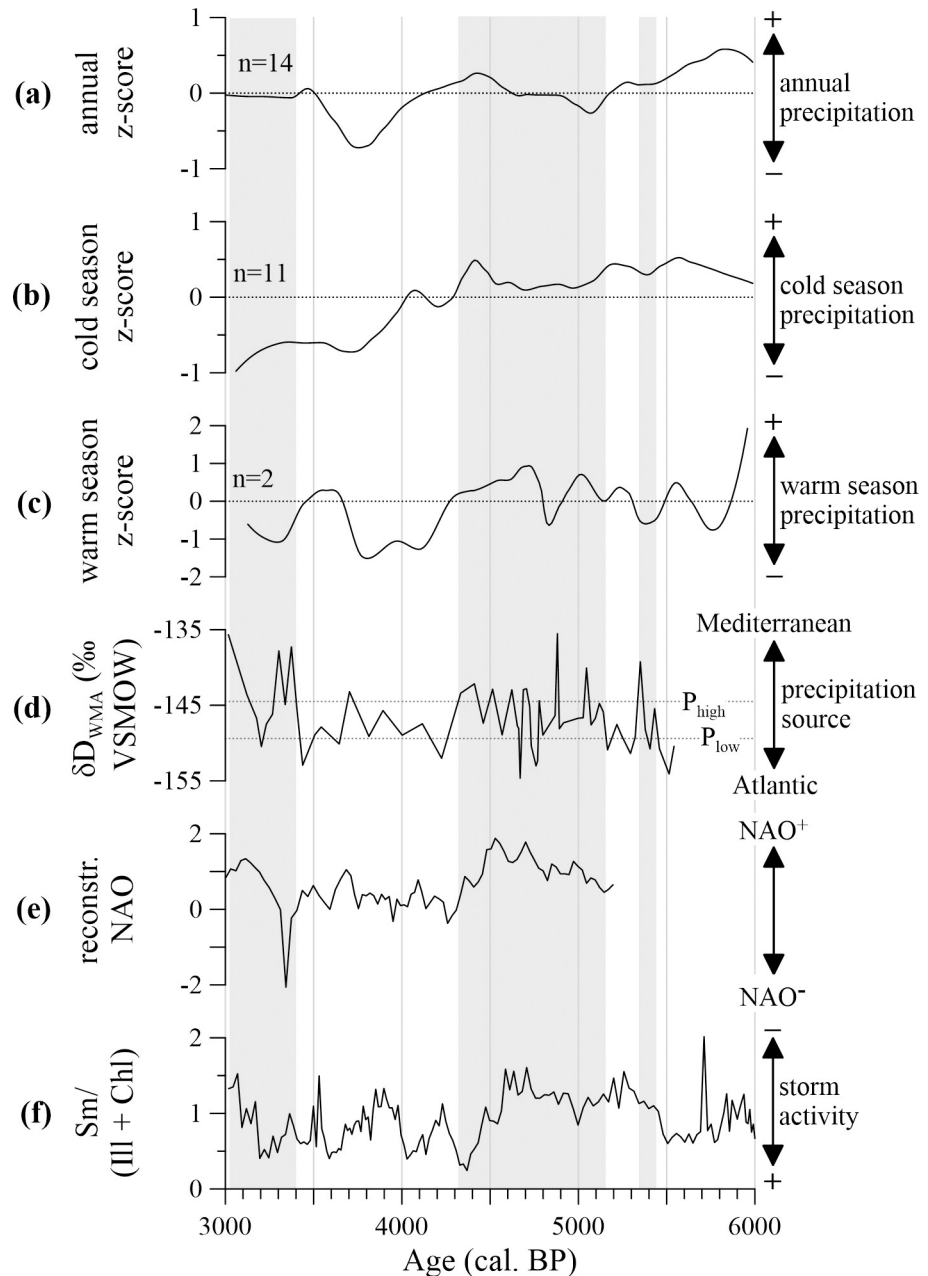


Fig 4. Atlantic versus Mediterranean influence. a) Regional z-score of annual precipitation variability, b) regional z-score of cold season precipitation variability, and c) regional z-score of warm season precipitation variability. Numbers of individual archives (n) included into the regional data are also shown. d) Weighted-mean average hydrogen isotopic data (δD_{WMA}) is displayed together with means of periods characterized by prolonged high (P_{high}) and low δD_{WMA} values (P_{low}) for orientation (see results-section). e) Reconstructed NAO from lake SS1200 in Greenland [87] and f) clay mineral ratio of Smectite (Sm), Illite (Ill), and Chlorite (Chl) from Gulf of Lions sediment core PB06 indicative of Western Mediterranean storminess [88] are shown for interpretation. Vertical grey bars indicate periods of increased Mediterranean precipitation in southeast Iberia based on the hydrogen isotopic data from ODP-161-976A.

<https://doi.org/10.1371/journal.pone.0243662.g004>

ODP-161-976A during the analysed period. Another potential driver is the source of precipitation [75]. Indeed, modern analyses of meteorological data from the Western Mediterranean indicate that δD_{prec} values in the area depend on the source of precipitation with Atlantic

Table 3. Correlation of paleoclimatological parameters from ODP-161-976A.

	$\delta D_{C_{29}}$	$\delta D_{C_{31}}$	$\delta D_{C_{33}}$	δD_{WMA}
$n-C_x$ conc.	R = 0.045	R = 0.084	R = 0.367	
	p = 0.725	p = 0.529	p = 0.004	
$\delta^{13}C_x$	R = 0.176	R = 0.363	R = 0.245	R = 0.310
	p = 0.196	p = 0.005	p = 0.073	p = 0.025
ACL ₂₉₋₃₅	R = 0.167	R = 0.281	R = 0.351	R = 0.377
	p = 0.206	p = 0.033	p = 0.007	p = 0.004
alkenone SST	R = 0.184	R = 0.114	R = 0.100	R = 0.195
	p = 0.160	p = 0.382	p = 0.440	p = 0.138

Correlation indices are given for the hydrogen isotopes of every individual n -alkane and their carbon isotopic values, their individual concentrations, cumulative concentration of long-chained odd n -alkanes, and the alkenone-based SST. Cross-plots of individual parameters are provided in the supplement of this article.

<https://doi.org/10.1371/journal.pone.0243662.t003>

derived precipitation exhibiting significantly lower δD_{prec} values compared to Mediterranean derived precipitation [48, 86]. Since Atlantic sourced precipitation in the study area is much more prominent during the winter season [30, 48], changes in precipitation source likely account for the apparent correlation of monthly amount-weighted δD_{prec} values with the monthly variability of atmospheric temperature and precipitation amount (Fig 1). n -Alkane δD values were also considered to reflect changes in the precipitation source by previous paleoclimatic studies from the Iberian Peninsula [65, 67, 68]. Accordingly, we conclude that the dominant parameter driving hydrogen isotopic variability of individual n -alkanes in marine sediment core ODP-161-976A is the source of precipitation with low δD_{WMA} values reflecting increasing Atlantic derived precipitation and high δD_{WMA} values reflecting an increase in Mediterranean sourced precipitation.

Over-regional driver of climate variability

Based on high δD_{WMA} values we define three major periods of overall enhanced Mediterranean sourced precipitation (Fig 4). These range from ca. 5450 to 5350 cal. BP, from 5150 to 4300 cal. BP including a short-term decrease in δD_{WMA} values around 4800 cal. BP, and from 3400 to 3000 cal. BP with an interruption around 3200 cal. BP. The latter two periods of enhanced Mediterranean sourced precipitation correspond well with times of dominant positive modes of the North Atlantic Oscillation (NAO⁺) [87] and reduced Western Mediterranean storminess [88, 89] (Fig 4). The Western Mediterranean storminess record, however, shows higher variability, which might be related to its distant location in the Gulf of Lions. But generally, NAO⁺ conditions would have favoured a northward shift of the Atlantic storm track towards northern and central Europe [43] (Fig 2). Consequently, this resulted in reduced storminess across the Western Mediterranean as generally evidenced by an increased clay mineral ratio from the Gulf of Lions during dominant positive NAO modes [88]. Along with the northward displacement of the Atlantic storm track, the majority of Atlantic sourced precipitation was shifted to northern and central Europe [90]. This results in high δD_{WMA} values as Atlantic sourced precipitation in southeast Iberia was reduced and the Mediterranean sourced precipitation gained more importance. One exception is observed at ca. 3350 cal. BP, when the NAO reconstruction indicates a prominent change to a negative mode (NAO⁻). These NAO⁻ conditions, however, represent a very abrupt, event-like feature, which might not be recorded in our data.

However, based on the modern NAO-precipitation relationship one would expect an increase in cold season precipitation when the Atlantic influence increases [24, 44]. Therefore,

it is interesting to note that the rapid shift in δD_{WMA} values towards relatively increased Atlantic moisture source at 4300 cal. BP is not coincident with elevated cold season precipitation levels (Fig 4). In fact, after 4300 cal. BP cold season precipitation at the south-eastern Iberian Peninsula reveals a prominent decreasing trend. Regarding the 4.2 ka BP event, which occurred during this period, previous studies indicate that this period was characterized by decreasing summer precipitation [6, 7, 28]. This is in line with our reconstruction of regional warm season precipitation, which indicates a rapid decrease between ca. 4200 to 3700 cal. BP (Fig 4). Taken into account that modern warm season precipitation in the area has a dominant Mediterranean source, a significant reduction in warm season precipitation might be able to explain the relative increase in Atlantic sourced precipitation at 4300 cal. BP, even though cold season precipitation was gradually decreasing.

According to the previous finding, a dominant role of the NAO—active during the cold season—as driver for the observed reduction in warm season precipitation during the 4.2 ka BP event is not plausible. However, based on *n*-alkane hydrogen isotopic analysis the Western Mediterranean Oscillation (WeMO) has recently been suggested as potential driver for changes in the precipitation source across southern Iberia during the studied period [68]. During modern times warm season precipitation at the southeast Iberian Peninsula is mainly derived from local convective systems [48], which benefit from a high land-sea temperature contrast (i.e. warm ocean and cool land). Such a high land-sea temperature contrast during the summer months is favoured by a positive mode of the Western Mediterranean Oscillation (WeMO⁺) due to the advection of cool air masses from the north [46, 48] (Fig 2). In contrast, WeMO⁻ conditions would favour a rather low land-sea temperature contrast because warm, easterly winds prevail [46]. Thus, our generally decreased δD_{WMA} data between 4300 and 3400 cal. BP along with the observed reduction in warm season precipitation could have been promoted by persistent WeMO⁻ conditions at that time.

Altogether, the NAO appears to be the dominant modulator of δD_{WMA} values, and thus, relative variability in moisture sources in the studied area between 6000 and 3000 cal. BP. This is plausible because annual precipitation is dominated by cold season precipitation on the Iberian Peninsula, which is also the season when the NAO is active [24]. However, secondary modes active during different seasons such as the WeMO may alter this overall relationship.

Conclusion

In order to investigate the interaction between Atlantic and Mediterranean climate at the south-eastern Iberian Peninsula during the mid- to late Holocene, compound-specific hydrogen (δD_{Cx}) and carbon isotopic records ($\delta^{13}C_{Cx}$) from fossil leaf waxes (i.e. *n*-alkanes) have been analysed. Detailed comparison with $\delta^{13}C_{Cx}$ values, sea surface temperature variability, and changes in precipitation amount indicate that δD_{Cx} values and their weighted-mean average (δD_{WMA}) analysed in this study are related to changes in the precipitation source. While low δD_{WMA} values are indicative of increased Atlantic origin, high δD_{WMA} values indicate a Mediterranean precipitation source.

Overall, δD_{WMA} variability appears closely related to variability of the North Atlantic Oscillation (NAO) between 6000 and 3000 cal. BP with positive NAO modes resulting in reduced storm activity across the Western Mediterranean and a relative increase of Mediterranean sourced precipitation in southeast Iberia. However, secondary atmospheric modes such as the Western Mediterranean Oscillation (WeMO) may alter this overall relationship. Such an example is the period of the 4.2 ka BP event, which on the southeast of the Iberian Peninsula was identified as a period of a rapid reduction in warm season precipitation between ca. 4200 and 3700 cal. BP. According to low δD_{WMA} values, these reductions in warm season

precipitation were related to a decreasing Mediterranean influence during the summer months. While it is not plausible that the NAO serves as driver for the reduced warm season precipitation, a hypothesized influence of the WeMO by lowering the land-sea temperature contrast is in line with a previous study [68].

Supporting information

S1 Fig. Cross-plots and correlations of environmental and paleoclimatological parameters of sediment core ODP-161-976A.

(TIF)

S2 Fig. Concentration of individual *n*-alkane homologues from sediment core ODP-161-976A.

(TIF)

Acknowledgments

This research was performed in the framework of the CRC 1266 “Scales of transformation”. Sample material has been provided by the IODP Core Repository at the MARUM—Center for Marine Environmental Sciences, University of Bremen, Germany. We thank Karsten Gramenz and Philipp Schindler for their enormous lab-work. We are grateful for the helpful reviews from Bülent Arıkan and Antonio García-Alix.

Author Contributions

Conceptualization: Julien Schirrmacher.

Data curation: Nils Andersen.

Formal analysis: Julien Schirrmacher.

Methodology: Julien Schirrmacher, Nils Andersen.

Project administration: Ralph R. Schneider, Mara Weinelt.

Resources: Ralph R. Schneider.

Supervision: Ralph R. Schneider, Mara Weinelt.

Visualization: Julien Schirrmacher.

Writing – original draft: Julien Schirrmacher.

Writing – review & editing: Nils Andersen, Ralph R. Schneider, Mara Weinelt.

References

1. Weiss H, Courty MA, Wetterstrom W, Guichard F, Senior L et al. (1993) The genesis and collapse of third millennium north mesopotamian civilization. *Science* (New York, N.Y.) 261 (5124): 995–1004. <https://doi.org/10.1126/science.261.5124.995> PMID: 17739617
2. Staubwasser M, Sirocko F, Grootes PM, Segl M (2003) Climate change at the 4.2 ka BP termination of the Indus valley civilization and Holocene south Asian monsoon variability. *Geophysical Research Letters* 30 (8): 155. Accessed 31 July 2017.
3. Welc F, Marks L (2014) Climate change at the end of the Old Kingdom in Egypt around 4200 BP. New ge archaeological evidence. *Quaternary International* 324: 124–133. Accessed 8 March 2018.
4. Liu F, Feng Z (2012) A dramatic climatic transition at ~4000 cal. yr BP and its cultural responses in Chinese cultural domains. *The Holocene* 22 (10): 1181–1197. Accessed 24 May 2018.
5. Valera AC (2015) Social change in the late 3rd millennium BC in Portugal: the twilight of enclosures. In: Meller H, Arz HW, Jung R, Risch R, editors. 2200 BC—ein Klimasturz als Ursache für den Zerfall der

- alten Welt. 7. Mitteldeutscher Archäologentag vom 23. bis 26. Oktober 2014 in Halle (Saale). Halle (Saale): Landesamt für Denkmalpflege und Archäologie Sachsen-Anhalt, Landesmuseum für Vorgeschichte. pp. 409–428.
6. Schirrmacher J, Kneisel J, Knitter D, Hamer W, Hinz M et al. (2020) Spatial patterns of temperature, precipitation, and settlement dynamics on the Iberian Peninsula during the Chalcolithic and the Bronze Age. *Quaternary Science Reviews* 233.
 7. Bini M, Zanchetta G, Perşoiu A, Cartier R, Català A et al. (2019) The 4.2 ka BP Event in the Mediterranean region. An overview. *Clim. Past* 15 (2): 555–577. Accessed 13 June 2019.
 8. Blanco-González A, Lillios KT, López-Sáez JA, Drake BL (2018) Cultural, Demographic and Environmental Dynamics of the Copper and Early Bronze Age in Iberia (3300–1500 BC). Towards an Interregional Multiproxy Comparison at the Time of the 4.2 ky BP Event. *J World Prehist* 31 (1): 1–79. Accessed 25 April 2018.
 9. Weiss H (2015) Megadrought, collapse, and resilience in late 3rd millennium BC Mesopotamia. In: Meller H, Arz HW, Jung R, Risch R, editors. 2200 BC—ein Klimasturz als Ursache für den Zerfall der alten Welt. 7. Mitteldeutscher Archäologentag vom 23. bis 26. Oktober 2014 in Halle (Saale). Halle (Saale): Landesamt für Denkmalpflege und Archäologie Sachsen-Anhalt, Landesmuseum für Vorgeschichte. pp. 35–52.
 10. Weiss H (2016) Global megadrought, societal collapse and resilience at 4.2–3.9 ka BP across the Mediterranean and west Asia. *PAGES Mag* 24 (2): 62–63.
 11. Schirrmacher J, Weinelt M, Blanz T, Andersen N, Salgueiro E et al. (2019) Multi-decadal atmospheric and marine climate variability in southern Iberia during the mid- to late-Holocene. *Clim. Past* 15 (2): 617–634. Accessed 19 June 2019.
 12. Kaniewski D, Marriner N, Cheddadi R, Guiot J, van Campo E (2018) The 4.2 ka BP event in the Levant. *Clim. Past* 14 (10): 1529–1542. Accessed 14 November 2018.
 13. Kathayat G, Cheng H, Sinha A, Berkelhammer M, Zhang H et al. (2018) Evaluating the timing and structure of the 4.2 ka event in the Indian summer monsoon domain from an annually resolved speleothem record from Northeast India. *Clim. Past* 14 (12): 1869–1879. Accessed 11 March 2019.
 14. Zhang H, Cheng H, Cai Y, Spötl C, Kathayat G et al. (2018) Hydroclimatic variations in southeastern China during the 4.2 ka event reflected by stalagmite records. *Clim. Past* 14 (11): 1805–1817. Accessed 11 March 2019.
 15. Giesche A, Staubwasser M, Petrie CA, Hodell DA (2019) Indian winter and summer monsoon strength over the 4.2 ka BP event in foraminifer isotope records from the Indus River delta in the Arabian Sea. *Clim. Past* 15 (1): 73–90.
 16. Booth RK, Jackson ST, Forman SL, Kutzbach JE, Bettis EA et al. (2005) A severe centennial-scale drought in midcontinental North America 4200 years ago and apparent global linkages. *The Holocene* 15 (3): 321–328.
 17. Bradley RS, Bakke J (2019) Is there evidence for a 4.2 ka BP event in the northern North Atlantic region. *Clim. Past* 15 (5): 1665–1676. Accessed 16 September 2020.
 18. Jalali B, Sicre M-A, Azuara J, Pellichero V, Combourieu-Nebout N (2019) Influence of the North Atlantic subpolar gyre circulation on the 4.2 ka BP event. *Clim. Past* 15 (2): 701–711. Accessed 1 October 2019.
 19. Geirsdóttir Á, Miller GH, Andrews JT, Harning DJ, Anderson LSet al. (2019) The onset of neoglaciation in Iceland and the 4.2 ka event. *Clim. Past* 15 (1): 25–40.
 20. Railsback LB, Liang F, Brook GA, Voarintsoa NRG, Sletten HR et al. (2018) The timing, two-pulsed nature, and variable climatic expression of the 4.2 ka event. A review and new high-resolution stalagmite data from Namibia. *Quaternary Science Reviews* 186: 78–90. Accessed 24 May 2018.
 21. Li H, Cheng H, Sinha A, Kathayat G, Spötl C et al. (2018) Speleothem Evidence for Megadroughts in the SW Indian Ocean during the Late Holocene. *Clim. Past Discuss.*: 1–23. Accessed 14 November 2018.
 22. Zielhofer C, Köhler A, Mischke S, Benkaddour A, Mikdad A et al. (2019) Western Mediterranean hydroclimatic consequences of Holocene ice-rafted debris (Bond) events. *Clim. Past* 15 (2): 463–475. Accessed 13 June 2019.
 23. Lionello P, editor (2012) *The climate of the Mediterranean region. From the past to the future.* Amsterdam: Elsevier Science. 502 p.
 24. Trigo RM, Pozo-Vázquez D, Osborn TJ, Castro-Díez Y, Gámiz-Fortis S et al. (2004) North Atlantic oscillation influence on precipitation, river flow and water resources in the Iberian Peninsula. *Int. J. Climatol* 24 (8): 925–944.

25. Zielhofer C, Fletcher WJ, Mischke S, Batist M de, Campbell JFE et al. (2017) Atlantic forcing of Western Mediterranean winter rain minima during the last 12,000 years. *Quaternary Science Reviews* 157: 29–51. Accessed 31 July 2017.
26. Ramos-Román MJ, Jiménez-Moreno G, Camuera J, García-Alix A, Anderson RS et al. (2018) Holocene climate aridification trend and human impact interrupted by millennial- and centennial-scale climate fluctuations from a new sedimentary record from Padul (Sierra Nevada, southern Iberian Peninsula). *Clim. Past* 14 (1): 117–137. Accessed 17 April 2018.
27. Yan M, Liu J (2019) Physical processes of cooling and mega-drought during the 4.2 ka BP event. Results from TraCE-21ka simulations. *Clim. Past* 15 (1): 265–277.
28. Baldini LM, Baldini JUL, McDermott F, Arias P, Cueto M et al. (2019) North Iberian temperature and rainfall seasonality over the Younger Dryas and Holocene. *Quaternary Science Reviews* 226: 105998. Accessed 27 February 2020.
29. Loidi J (2017) *The Vegetation of the Iberian Peninsula*. Cham: Springer International Publishing.
30. Fick SE, Hijmans RJ (2017) WorldClim 2. New 1-km spatial resolution climate surfaces for global land areas. *Int. J. Climatol.* 37 (12): 4302–4315.
31. Ilvonen L, López-Sáez JA, Holmström L, Alba-Sánchez F, Pérez-Díaz S et al. (2019) Quantitative reconstruction of precipitation changes in the Iberian Peninsula during the Late Pleistocene and the Holocene. *Clim. Past Discuss.*: 1–30.
32. Jones SE, Burjachs F, Ferrer-García C, Giral S, Schulte L et al. (2018) A multi-proxy approach to understanding complex responses of salt-lake catchments to climate variability and human pressure. A Late Quaternary case study from south-eastern, Spain. *Quaternary Science Reviews* 184: 201–223. Accessed 13 June 2019.
33. Burjachs F, Giral S, Roca JR, Seret G, Julià R (1997) Palinología holocénica y desertización en el Mediterráneo occidental. In: Ibañez JJ, Valero BL, Machado C, editors. *El paisaje mediterráneo a través del espacio y del tiempo. Implicaciones en la desertificación*. Logroño: Geoforma Editores. pp. 379–394.
34. Pantaléon-Cano J, Yll E-I, Pérez-Obiol R, Roure JM (2003) Palynological evidence for vegetational history in semi-arid areas of the western Mediterranean (Almería, Spain). *The Holocene* 13 (1): 109–119. Accessed 24 May 2018.
35. Carrión JS, Sánchez-Gómez P, Mota JF, Yll R, Chaín C (2003) Holocene vegetation dynamics, fire and grazing in the Sierra de Gádor, southern Spain. *The Holocene* 13 (6): 839–849. Accessed 31 July 2017.
36. Burjachs F, Expósito I (2015) Charcoal and pollen analysis. Examples of Holocene fire dynamics in Mediterranean Iberian Peninsula. *CATENA* 135: 340–349. Accessed 31 July 2017.
37. Walczak IW, Baldini JUL, Baldini LM, McDermott F, Marsden S et al. (2015) Reconstructing high-resolution climate using CT scanning of unsectioned stalagmites. A case study identifying the mid-Holocene onset of the Mediterranean climate in southern Iberia. *Quaternary Science Reviews* 127: 117–128. Accessed 2 August 2017.
38. Cortés-Sánchez M, Morales-Muñiz A, Simón-Vallejo MD, Lozano-Francisco MC, Vera-Peláez JL et al. (2011) Earliest known use of marine resources by Neanderthals. *PloS one* 6 (9): e24026. <https://doi.org/10.1371/journal.pone.0024026> PMID: 21935371
39. Combourieu Nebout N, Peyron O, Dormoy I, Desprat S, Beaudouin C et al. (2009) Rapid climatic variability in the west Mediterranean during the last 25 000 years from high resolution pollen data. *Clim. Past* 5 (1): 671–707. Accessed 12 October 2018.
40. Fletcher WJ, Sanchez Goñi MF, Peyron O, Dormoy I (2010) Abrupt climate changes of the last deglaciation detected in a Western Mediterranean forest record. *Clim. Past* 6 (2): 245–264. Accessed 14 November 2018.
41. Fletcher WJ, Sánchez Goñi MF (2008) Orbital- and sub-orbital-scale climate impacts on vegetation of the western Mediterranean basin over the last 48,000 yr. *Quat. res.* 70 (03): 451–464. Accessed 17 April 2018.
42. Peyron O, Combourieu-Nebout N, Brayshaw D, Goring S, Andrieu-Ponel V et al. (2017) Precipitation changes in the Mediterranean basin during the Holocene from terrestrial and marine pollen records. A model–data comparison. *Climate of the Past* 13 (3): 249–265. Accessed 28 July 2017.
43. Hurrell JW (1995) Decadal trends in the north atlantic oscillation: regional temperatures and precipitation. *Science* 269 (5224): 676–679. <https://doi.org/10.1126/science.269.5224.676> PMID: 17758812
44. Hernández A, Trigo RM, Pla-Rabes S, Valero-Garcés BL, Jerez S et al. (2015) Sensitivity of two Iberian lakes to North Atlantic atmospheric circulation modes. *Clim Dyn* 45 (11–12): 3403–3417. Accessed 1 October 2018.
45. Martin-Vide J, Lopez-Bustins J-A (2006) The Western Mediterranean Oscillation and rainfall in the Iberian Peninsula. *Int. J. Climatol.* 26 (11): 1455–1475. Accessed 18 January 2018.

46. Lopez-Bustins JA, Lemus-Canovas M (2020) The influence of the Western Mediterranean Oscillation upon the spatio-temporal variability of precipitation over Catalonia (northeastern of the Iberian Peninsula). *Atmospheric Research* 236: 104819. Accessed 25 August 2020.
47. Barnston AG, Livezey RE (1987) Classification, Seasonality and Persistence of Low-Frequency Atmospheric Circulation Patterns. *Mon. Wea. Rev.* 115 (6): 1083–1126.
48. Araguas-Araguas LJ, Diaz Teijeiro MF (2005) Isotope composition of precipitation and water vapour in the Iberian Peninsula. In: International Atomic Energy Agency, editor. *Isotopic composition of precipitation in the Mediterranean basin in relation to air circulation patterns and climate. Final report of a coordinated research project 2000–2004.* Vienna: IAEA. pp. 173–190.
49. Gimeno L, Nieto R, Trigo RM, Vicente-Serrano SM, López-Moreno JI (2010) Where Does the Iberian Peninsula Moisture Come From. An Answer Based on a Lagrangian Approach. *Journal of Hydrometeorology* 11 (2): 421–436. Accessed 25 August 2020.
50. Eglinton G, Hamilton RJ (1967) Leaf Epicuticular Waxes. *Science* 156 (3780): 1322–1335. <https://doi.org/10.1126/science.156.3780.1322> PMID: 4975474
51. Bird MI, Summons RE, Gagan MK, Roksandic Z, Dowling L et al. (1995) Terrestrial vegetation change inferred from n-alkane $\sigma^{13}\text{C}$ analysis in the marine environment. *Geochimica et Cosmochimica Acta* 59 (13): 2853–2857. Accessed 4 June 2018.
52. Conte MH, Weber JC (2002) Long-range atmospheric transport of terrestrial biomarkers to the western North Atlantic. *Global Biogeochem. Cycles* 16 (4): 89–1–89–17. Accessed 4 June 2018.
53. Schreuder LT, Stuu J-BW, Korte LF, Sinnighe Damsté JS, Schouten S (2018) Aeolian transport and deposition of plant wax n-alkanes across the tropical North Atlantic Ocean. *Organic Geochemistry* 115: 113–123. Accessed 25 May 2018.
54. Schimmelmann A, Sessions AL, Mastalerz M (2006) Hydrogen isotopic (D/H) composition of organic matter during diagenesis and thermal maturation. *Annu. Rev. Earth Planet. Sci.* 34 (1): 501–533.
55. Wang C, Eley Y, Oakes A, Hren M (2017) Hydrogen isotope and molecular alteration of n-alkanes during heating in open and closed systems. *Organic Geochemistry* 112: 47–58.
56. Bray EE, Evans ED (1961) Distribution of n-paraffins as a clue to recognition of source beds. *Geochimica et Cosmochimica Acta* 22 (1): 2–15.
57. Bush RT, McInerney FA (2013) Leaf wax n-alkane distributions in and across modern plants. Implications for paleoecology and chemotaxonomy. *Geochimica et Cosmochimica Acta* 117: 161–179. Accessed 31 July 2017.
58. Norström E, Katrantsiotis C, Smittenberg RH, Kouli K (2017) Chemotaxonomy in some Mediterranean plants and implications for fossil biomarker records. *Geochimica et Cosmochimica Acta* 219: 96–110. Accessed 25 May 2018.
59. Leider A, Hinrichs K-U, Schefuß E, Versteegh GJM (2013) Distribution and stable isotopes of plant wax derived n-alkanes in lacustrine, fluvial and marine surface sediments along an Eastern Italian transect and their potential to reconstruct the hydrological cycle. *Geochimica et Cosmochimica Acta* 117: 16–32. Accessed 31 July 2017.
60. García-Alix A, Jiménez-Espejo FJ, Toney JL, Jiménez-Moreno G, Ramos-Román MJ et al. (2017) Alpine bogs of southern Spain show human-induced environmental change superimposed on long-term natural variations. *Scientific reports* 7 (1): 7439. Accessed 18 October 2017. <https://doi.org/10.1038/s41598-017-07854-w> PMID: 28785039
61. Schefuß E, Schouten S, Schneider RR (2005) Climatic controls on central African hydrology during the past 20,000 years. *Nature* 437 (7061): 1003–1006. Accessed 31 July 2017. <https://doi.org/10.1038/nature03945> PMID: 16222296
62. Niedermeyer EM, Schefuß E, Sessions AL, Mulitza S, Mollenhauer G et al. (2010) Orbital- and millennial-scale changes in the hydrologic cycle and vegetation in the western African Sahel. Insights from individual plant wax δD and $\delta^{13}\text{C}$. *Quaternary Science Reviews* 29 (23–24): 2996–3005. Accessed 31 July 2017.
63. Niedermeyer EM, Forrest M, Beckmann B, Sessions AL, Mulch A et al. (2016) The stable hydrogen isotopic composition of sedimentary plant waxes as quantitative proxy for rainfall in the West African Sahel. *Geochimica et Cosmochimica Acta* 184: 55–70. Accessed 31 July 2017.
64. Kuechler RR, Schefuß E, Beckmann B, Dupont L, Wefer G (2013) NW African hydrology and vegetation during the Last Glacial cycle reflected in plant-wax-specific hydrogen and carbon isotopes. *Quaternary Science Reviews* 82: 56–67. Accessed 31 July 2017.
65. Taylor AK, Benedetti MM, Haws JA, Lane CS (2018) Mid-Holocene Iberian hydroclimate variability and paleoenvironmental change. Molecular and isotopic insights from Praia Rei Cortiço, Portugal. *J. Quaternary Sci.* 33 (1): 79–92. Accessed 29 May 2018.

66. Schemmel F, Niedermeyer EM, Schwab VF, Gleixner G, Pross J et al. (2016) Plant wax δD values record changing Eastern Mediterranean atmospheric circulation patterns during the 8.2 kyr B.P. climatic event. *Quaternary Science Reviews* 133: 96–107. Accessed 31 July 2017.
67. Schäfer IK, Bliedtner M, Wolf D, Kolb T, Zech J et al. (2018) A $\delta^{13}C$ and δ^2H leaf wax record from the Late Quaternary loess-paleosoil sequence El Paraiso, Central Spain. *Palaeogeography, Palaeoclimatology, Palaeoecology* 507: 52–59. Accessed 1 October 2018.
68. Toney JL, García-Alix A, Jiménez-Moreno G, Anderson RS, Moossen H et al. (2020) New insights into Holocene hydrology and temperature from lipid biomarkers in western Mediterranean alpine wetlands. *Quaternary Science Reviews* 240: 106395. Accessed 22 June 2020.
69. Diefendorf AF, Freimuth EJ (2017) Extracting the most from terrestrial plant-derived n-alkyl lipids and their carbon isotopes from the sedimentary record. A review. *Organic Geochemistry* 103: 1–21. Accessed 29 May 2018.
70. Schwab VF, Garcin Y, Sachse D, Todou G, Séné O et al. (2015) Effect of aridity on $\delta^{13}C$ and δD values of C_3 plant- and C_4 graminoid-derived leaf wax lipids from soils along an environmental gradient in Cameroon (Western Central Africa). *Organic Geochemistry* 78: 99–109. Accessed 31 July 2017.
71. Farquhar GD, O'Leary MH, Berry JA (1982) On the Relationship Between Carbon Isotope Discrimination and the Intercellular Carbon Dioxide Concentration in Leaves. *Functional Plant Biol.* 9 (2): 121.
72. Wang YV, Larsen T, Leduc G, Andersen N, Blanz T et al. (2013) What does leaf wax δD from a mixed C_3/C_4 vegetation region tell us. *Geochimica et Cosmochimica Acta* 111: 128–139. Accessed 8 March 2018.
73. Gamarra B, Sachse D, Kahmen A (2016) Effects of leaf water evaporative 2H -enrichment and biosynthetic fractionation on leaf wax n-alkane δ^2H values in C_3 and C_4 grasses. *Plant, Cell and Environment* 39 (11): 2390–2403. Accessed 31 July 2017. <https://doi.org/10.1111/pce.12789> PMID: 27392279
74. Sachse D, Billault I, Bowen GJ, Chikaraishi Y, Dawson TE et al. (2012) Molecular Paleohydrology. Interpreting the Hydrogen-Isotopic Composition of Lipid Biomarkers from Photosynthesizing Organisms. *Annual Review of Earth and Planetary Sciences* 40 (1): 221–249. Accessed 31 July 2017.
75. Wirth SB, Sessions AL (2016) Plant-wax D/H ratios in the southern European Alps record multiple aspects of climate variability. *Quaternary Science Reviews* 148: 176–191. Accessed 31 July 2017.
76. Dansgaard W (1964) Stable isotopes in precipitation. *Tellus* 16 (4): 436–468. Accessed 27 February 2020.
77. Comas MC, Zahn R, Klaus A, editors (1996) Proceedings of the Ocean Drilling Program, 161 Initial Reports: Ocean Drilling Program.
78. Gouveia C, Trigo RM, DaCamara CC, Libonati R, Pereira JMC (2008) The North Atlantic Oscillation and European vegetation dynamics. *Int. J. Climatol.* 28 (14): 1835–1847.
79. Cariñanos P, Galan C, Alcázar P, Domínguez E (2004) Airborne pollen records response to climatic conditions in arid areas of the Iberian Peninsula. *Environmental and Experimental Botany* 52 (1): 11–22. Accessed 16 January 2020.
80. Clark-Carter D (2014) z Scores. In: Balakrishnan N, editor. Wiley StatsRef. Statistics Reference Online. [Erscheinungsort nicht ermittelbar]: Wiley. p. 44.
81. Garcin Y, Schwab VF, Gleixner G, Kahmen A, Todou G et al. (2012) Hydrogen isotope ratios of lacustrine sedimentary n-alkanes as proxies of tropical African hydrology. Insights from a calibration transect across Cameroon. *Geochimica et Cosmochimica Acta* 79: 106–126. Accessed 31 July 2017.
82. Collins JA, Schefuß E, Mulitza S, Prange M, Werner M et al. (2013) Estimating the hydrogen isotopic composition of past precipitation using leaf-waxes from western Africa. *Quaternary Science Reviews* 65: 88–101. Accessed 31 July 2017.
83. Nelson DM, Henderson AK, Huang Y, Hu FS (2013) Influence of terrestrial vegetation on leaf wax δD of Holocene lake sediments. *Organic Geochemistry* 56: 106–110. Accessed 31 July 2017.
84. Sachse D, Radke J, Gleixner G (2006) δD values of individual n-alkanes from terrestrial plants along a climatic gradient—Implications for the sedimentary biomarker record. *Organic Geochemistry* 37 (4): 469–483. Accessed 31 July 2017.
85. Struck J, Bliedtner M, Strobel P, Schumacher J, Bazarradnaa E et al. (2020) Leaf wax n-alkane patterns and compound-specific $\delta^{13}C$ of plants and topsoils from semi-arid and arid Mongolia. *Biogeosciences* 17 (3): 567–580. Accessed 16 September 2020.
86. Ouda B, El Hamdaoui M, Ibn Majah M (2005) Isotopic composition of precipitation at three Moroccan stations influenced by Oceanic and Mediterranean air masses. In: International Atomic Energy Agency, editor. Isotopic composition of precipitation in the Mediterranean basin in relation to air circulation patterns and climate. Final report of a coordinated research project 2000–2004. Vienna: IAEA. pp. 125–140. <https://doi.org/10.1079/bjn20051445> PMID: 16115329

87. Olsen J, Anderson NJ, Knudsen MF (2012) Variability of the North Atlantic Oscillation over the past 5,200 years. *Nature Geoscience* 5 (11): 808–812. Accessed 31 July 2017.
88. Sabatier P, Dezileau L, Colin C, Briquet L, Bouchette F et al. (2012) 7000 years of paleostorm activity in the NW Mediterranean Sea in response to Holocene climate events. *Quat. res.* 77 (01): 1–11. Accessed 30 August 2017.
89. Dezileau L, Pérez-Ruzafa A, Blanchemanche P, Degeai J-P, Raji O et al. (2016) Extreme storms during the last 6500 years from lagoonal sedimentary archives in the Mar Menor (SE Spain). *Clim. Past* 12 (6): 1389–1400. Accessed 29 May 2018.
90. Trigo RM, Osborn TJ, Corte-Real JM (2002) The North Atlantic Oscillation influence on Europe. *Climate impacts and associated physical mechanisms.* *Clim. Res.* 20: 9–17. Accessed 2 October 2018.